Human embryonic stem cells and metastatic colorectal cancer cells shared the common endogenous human microRNA-26b

Yan-Lei Ma [a, #]**, Peng Zhang** [a, #]**, Feng Wang** [a, #]**, Mary Pat Moyer** [b]**, Jian-Jun Yang** [a]**, Zhi-Hua Liu** [a]**,
Jia-Yuan Peng** [a]**, Hong-Qi Chen** [a]**, Yu-Kun Zhou** [a]**, Wei-Jie Liu** [a]**, Huan-Long Qin** [a, *]

[a] *Department of Surgery, The Sixth People's Hospital Affiliated to Shanghai Jiao Tong University,
Shanghai, People's Republic of China*
[b] *INCELL Corporation, San Antonio, TX, USA*

Abstract

The increase in proliferation and the lack of differentiation of cancer cells resemble what occur in the embryonic stem cells during physiological process of embryogenesis. There are also striking similarities in the behaviour between the invasive placental cells and invasive cancer cells. In the present study, microarrays were used to analyse the global expression of microRNAs in a human embryonic stem cell line (*i.e.* HUES-17) and four colorectal cancer (CRC) cell lines (*i.e.* LoVo, SW480, HT29 and Caco-2) with different metastatic potentialities. Only the expression of miR-26b was significant decreased in HUES-17s and LoVo cells, compared with other three cell lines ($P < 0.01$). The quantitative real-time PCR analysis confirmed the results of the microarray analysis. Overexpression of miR-26b expression by miR-26 mimics transfection and led to the significant suppression of the cell growth and the induction of apoptosis in LoVo cells *in vitro*, and the inhibition of tumour growth *in vivo*. Moreover, the potential targets of miR-26b was predicted by using bioinformatics, and then the predicted target genes were further validated by comparing gene expression profiles between LoVo and NCM460 cell lines. Four genes (TAF12, PTP4A1, CHFR and ALS2CR2) with intersection were found to be the targets of miR-26b. MetaCore network analysis further showed that the regulatory pathways of miR-26b were significantly associated with the invasiveness and metastasis of CRC cells. These data suggest that miR-26b might serve as a novel prognostic factor and a potential therapeutic target for CRC.

Keywords: colorectal cancer ● human embryonic stem cells ● metastatic colorectal cancer cells ● miR-26b

Introduction

MicroRNAs (miRNAs) are an abundant class of endogenous, single-stranded, small non-coding RNAs found in diverse organisms [1]. The number of verified human miRNAs is still expanding. They negatively regulate the translation of specific mRNAs by base pairing with partially or fully complementary sequences in target mRNAs [2–4]. Many miRNAs are evolutionarily conserved and have well-defined developmental and cell type specific expression patterns [5]. It is well known today that miRNAs have very impor-

tant regulatory functions in such basic biological processes as development, cellular differentiation, gene regulation, proliferation and apoptosis that affect such major biological systems as stemness, immunity and cancer development [6–9].

Although metastasis is the main reason for mortality in patients with solid tumours, our understanding of its molecular and cellular determinants is still limited [10–13]. Recently, several experimental studies have demonstrated sets of genes, or 'signatures' that could program many of the cell–biological changes needed to execute the initial steps of the invasion–metastasis cascade [14–19]. However, much less insight has been gained into the regulatory networks that establish such altered gene expression states [20]. miRNAs are attractive candidates as upstream regulators of metastatic progression because they could post-transcriptionally regulate entire sets of genes [21]. Recent studies have indicated that some miRNAs may play an important role in the early development of carcinogenesis as either oncogenes or

[#]These authors contributed equally.
[*]Correspondence to: Huan-Long QIN,
Department of Surgery, The Sixth People's Hospital Affiliated
to Shanghai Jiao Tong University, 600 Yishan Road,
Shanghai 200233, People's Republic of China.
Tel.: +86 21 64361349
Fax: +86 21 64368920
E-mail: hl-qin@hotmail.com

tumour suppressor genes [7, 22–23]. Moreover, a few miRNAs may act at late stages of tumour progression, and the characteristic miRNA signatures in certain human cancers have revealed unique expression profiles [24–26]. However, which miRNAs are associated with, or regulate tumour progression remains unclear.

Our reported in our previous study on the potential oncofoetal biomarker desmin for colorectal cancer (CRC) [27], provides support for the hypothesis that tumorigenesis and embryogenesis are postulated to share certain common pathways [28–29]. For example, the increase in proliferation and the lack of differentiation of cancer cells resemble what occur in the embryonic stem cells during the physiological process of embryogenesis [30]. There are also striking similarities in the behaviour between invasive placental cells and invasive cancer cells [28]. The cellular mechanisms used by the cells of the placenta during implantation are reused by cancer cells during the invasiveness and metastasis within the body. In addition, miRNAs are necessary for stem cell division, cell fate determination and patterning in early and later stages of development, in which they regulate cell differentiation and maintain the pluripotent cell state [31–32]. Overlapping expression of miRNAs in human embryonic colon and CRC were also found in the experimental study [30]. The sequences of many miRNAs are conserved among distantly related organisms, suggesting that these molecules participate in essential processes, including normal embryonic development and carcinogenesis [7, 33].

In the present study, microarrays were used to analyse the global expression of miRNAs in a human embryonic stem cell (hESC) line (*i.e.* HUES-17) and four CRC cell lines (*i.e.* LoVo, SW480, HT29 and Caco-2) with different metastatic potentialities. We postulate that hESCs and tumour metastasis cells, especially those with a high metastatic potentiality, may share some common endogenous miRNAs, and these miRNAs may modulate the expression of certain gene products of signalling pathways that are involved in both embryo implantation (or intestinal development) and progression in CRC.

Materials and methods

Cell culture

HUES-17, a hESC line, was provided by the Melton Laboratory, Harvard University. The experiments on hESCs were approved by the ethical committee of the Sixth People's Hospital Affiliated to Shanghai Jiao Tong University, and conducted in accordance with the Guidelines for Research on hESCs, jointly issued by the Ministry of Science and Technology and the Ministry of Health of China. HUES-17 cells were cultured on feeders in a medium containing 80% Dulbecco's modified Eagle's medium/Ham's F-12 medium (Invitrogen, New York, NY, USA), 20% knockout serum replacement, 1 mM L-glutamine, 0.1 mM β-mercaptoethanol, 1% non-essential amino acids and 4 ng/ml human basic fibroblast growth factor. Protein factors or SB431542, a small molecule inhibitor, were added directly to the culture in the continuous presence of the conditioned medium [34].

One CRC cell line with a high metastatic potential LoVo and three CRC cell lines, *i.e.* LoVo, SW480, HT29 and Caco-2, with a low metastatic potential were obtained from the American Type Culture Collection (ATCC, Manassas, VA, USA). CRC cells were cultured in serum-containing medium at a density of 1×10^5 cells/ml. LoVo, SW480, HT29 and Caco-2 were, respectively, maintained in their preferred growth media Ham's F-12 medium with Kaighn's modification (F12K), Roswell Park Memorial Institute 1640 (RPMI1640) medium, ATCC-formulated McCoy's 5a medium and Dulbecco's modified Eagle's medium. All media were supplemented with 10% v/v foetal bovine serum (FBS; Invitrogen) in a humidified 5% CO_2 atmosphere at 37°C.

RNA extraction

Total RNA was extracted from the five cell lines by using Qiagen RNeasy kit (QIAGEN, Hilden, Germany) according to the manufacturer's instructions. Total RNA was quantified by microfluidic analysis.

μParaflo™ microRNA microarray assay

μParaflo™ MicroRNA Microarray (release 13.0) assay was performed by LC Sciences (Houston, TX, USA). The assay started from 2 to 5 μg total RNA samples, which was size fractionated by using a YM-100 Microcon centrifugal filter (Millipore Corp., Billerica, MA, USA), and the small RNAs (<300 nt) isolated were 3′-extended with a poly(A) tail by using poly(A) polymerase. An oligonucleotide tag was then ligated to the poly(A) tail for later fluorescent dye staining. Hybridization was performed overnight on a μParaflo™ microfluidic chip by using a micro-circulation pump (Atactic Technologies, Inc., Houston, TX, USA) [35]. On the microfluidic chip, each detection probe consisted of a chemically modified nucleotide coding segment complementary to the target miRNA (from miRBase, http://microrna.sanger.ac.uk/sequences/) and a spacer segment of polyethylene glycol to extend the coding segment away from the substrate. The hybridization melting temperatures were balanced by chemical modifications of the detection probes. Hybridization was performed in 100 μl 6× SSPE buffer (0.90 M NaCl, 60 mM Na_2HPO_4, 6 mM ethylenediaminetetraacetic acid, pH 6.8) containing 25% formamide at 34°C. After hybridization, tag-specific Cy5 dyes were used for fluorescence labelling. Hybridization images were collected with a laser scanner (GenePix 4000B, Molecular Device, Sunnyvale, CA, USA) and digitized with Array-Pro image analysis software (Media Cybernetics, Bethesda, MD, USA).

Normalization and data analysis of microarray data

MiRNA microarray data were analysed by first subtracting the background and then normalizing the signals with a LOWESS filter (locally weighted regression) as described previously [36]. Differentially expressed miRNAs were defined when the *P*-value was less than 0.05, and most notable differentially expressed miRNAs were defined when the *P*-value was less than 0.01. In the present study, only those most notable differentially expressed miRNAs were further investigated in confirmatory and validation experiments as described below. Dendrograms and expression maps were generated by the Treeview version 1.6 program (Department of Genetics, Stanford University School of Medicine, Stanford, CA, USA) [37].

Confirmation and validation of most notable differentially expressed miRNA(s) with quantitative real-time PCR for miRNA analysis

To confirm the microarray results, the most notable differentially expressed miRNAs, as determined by the microarray with a *P*-value of less than 0.01, were further investigated by using TaqMan real-time PCR in the five cell lines, according to the instructions of the manufacturer (Applied Biosystems, Foster, CA, USA). In addition, quantitative real-time PCR (qRT-PCR) was performed on the 7000 Real-Time PCR system (Applied Biosystems) by using miRNA-specific primers provided with the Applied Biosystems TaqMan MicroRNA Assay kit. For each reaction, 10 μl 2× TaqMan universal PCR master mix, 1 μl 20× TaqMan MicroRNA primers and 1 μl real-time PCR product (10-fold dilution from PCR reaction) and 8 μl nuclease free water were added, with the final volume of 20 μl. The qRT-PCR reactions were performed in a 96-well optical microplate at 95°C for 10 min., followed by 40 cycles of 95°C for 15 sec. (to denature DNA) and 60°C for 60 sec. (for primer annealing and extending). In qRT-PCR, small nucleolar RUN24 served as an endogenous reference gene for normalizing the content of qRT-PCR products. Relative miRNA expression data were analysed by using the $2^{-\Delta CT}$ method. All assays were performed in triplicate.

To validate the microarray results *in vivo*, fresh CRC and paired normal colorectal tissues from 9 patients and colorectal adenoma tissues from 10 patients were obtained by experienced surgeons and examined by experienced pathologists at Sixth People's Hospital, Shanghai Jiao Tong University. The study protocol was approved by the Scientific and Ethical Committee of Shanghai Jiao Tong University. Then, miRNA-26b expression was determined by qRT-PCR as described above.

Cell transfection

The human CRC cell line LoVo was grown in F12k medium with 10% FBS in a humidified atmosphere containing 5% CO_2 at 37°C. Then, the cells were transfected with miR-26b mimics (Shanghai GenePharma Corp., Shanghai, China) or a miR-26b mimics control, short double-stranded RNAs similar to Dicer-processed miRNAs [38], using Lipofectamine 2000 (Invitrogen, Carlsbad, CA, USA), The combinations were transfected to the cells in indicated concentrations according to the manufacturer's recommendation.

Quantitative real-time PCR for miR-26b in transfected LoVo cells with miR-26b mimics

Total RNA was extracted from the cells using TRIzol (Invitrogen) according to the manufacturer's instructions. First-strand complementary DNA was synthesized from 2 μg of total RNA using an oligo-dT primer and super-script II reverse transcriptase (Invitrogen). To quantify miR-26b real-time PCR, using SYBR® Premix Ex Taq™ (TakaRa BIO INC., Otsu, Shiga, Japan) was done with the following primer pairs; Primers for miR-26b were 5′-GAGAGGTATGAAGGTTATTCA-3′ for forward and 5′-ATCACCACCTTAC-GAGCCACC-3′ for reverse. The primers for U6 (TakaRa BIO INC.), which was used as an internal control, were 5′- CGCTTCGGCAGCACATATAC-3′ for forward and 5′- TTCACGAATTTGCGTGTCAT-3′ for reverse. PCR was performed in a real-time PCR system (BIO-RAD, Berkeley, CA, USA) as

follows: 95°C for 3 min. followed by 35 cycles of 95°C for 5 sec., 60°C for 20 sec. and 72°C for 30 sec., and then 94°C for 1 min., 60°C 1 min., add a cycle every 0.5 degrees. Expression values normalized to those for U6. Relative fold changes of miR-26b expression were calculated by the ΔCT method, and the values were expressed as $2^{-\Delta CT}$.

Clonogenic formation assay

miR-26b mimics-treated and miR-26b mimics control-treated LoVo cells (1×10^4) were seeded in 10 cm dishes. Two weeks later, cells were washed with phosphate-buffered saline (PBS), stained with 0.5% w/v crystal violet in 20% methanol (Sigma-Aldrich, St. Louis, MO, USA), and the number of colonies was counted after 20 min.

Flow cytometry analysis

Apoptosis was assessed by measuring the membrane redistribution of phosphatidylserine with an annexin V-PI (propidium iodide) apoptosis detection kit (Sigma-Aldrich). According to the manufacturer's protocol, cells were harvested by trypsinization and rinsed with cold PBS twice 48 hrs after transfection. After centrifugation ($1000 \times g$ at 4°C) for 5 min., cells were suspended in PBS twice, with centrifugation. Each sample tube had 80 μl PBS added followed by 100 μl staining buffer (1× PBS, 20 μl PI, 0.4 μl RNase). After vortexing, samples were placed in the water bath at 37°C for 30 min. Each sample had 400 μl PBS added and apoptosis was measured by flow cytometric analysis with a combination of annexin V and propidiumiodide.

Cell migration and invasion assays

Cell migration and invasion were detected by using Transwell chambers (8 mm, Corning Costar Co., Lowell, MA, USA). miR-26b mimics-treated and miR-26b mimics control-treated LoVo cells (5×10^4) in 400 μl of serum-free F12k medium were placed in the uncoated (migration assay) or 1:10 diluted Matrigel®-coated (invasion assay) upper chamber. The lower chamber was filled with 1 ml of complete F12k medium. After an incubation period of 12 hrs at 37°C, the cells on the upper surface of the filter that had migrated to the bottom surface of the membrane were fixed and stained with 0.5% crystal violet solution. Cells on the top surface of the membrane were removed by wiping with a cotton swab. Cells adhering to the bottom surface of the filter that were fixed and stained with 0.5% crystal violet solution were counted in five randomly selected microscopic fields (×200). Three independent experiments were carried out, with each in triplicate.

Preparation of liposomal miR-26b mimics and liposomal mimics control

miR-26b mimics or miR-26b mimics control for *in vivo* delivery was either given naked (without transfection agent), or incorporated into dioleoylphosphatidylcholine (DOPC, Roche, Basel, Switzerland), and miR-26b mimics were mixed in the presence of excess tertiary butanol (t-butanol) (Sigma-Aldrich) at a ratio of 1:10 (w/w) siRNA/DOPC. Tween 20 (Sigma-Aldrich) was added to the mixture in a ratio of 1:19 Tween 20:

siRNA/DOPC. The mixture was vortexed, frozen in an acetone/dry ice bath and lyophilized. Before *in vivo* administration, this preparation was hydrated with normal 0.9% saline at a concentration of 15 μg/ml to achieve the desired dose in 150 to 200 μl per injection. To estimate the quantity of siRNA not taken up by liposomes, free siRNA was separated from liposomes using 30,000 nominal molecular weight limit filter units (Millipore Corp.). The liposomal suspension was added to the filters and centrifuged at 5000 × *g* for 40 min. at room temperature. Fractions were collected, the material trapped in the filter was reconstituted with 0.9% saline, and siRNA of the collected fraction and the elute was measured by spectrophotometry.

Xenograft experiments

All animal experiments were approved by the Ethics Committee for Animal Use of the Sixth People's Hospital Affiliated to Shanghai Jiao-Tong University. Healthy female nude mice (BALB/C, Chinese Academy of Sciences, Shanghai, China), 6–8 weeks of age, infertile and 18–20 g, were injected subcutaneously with LoVo cells ($2 \times 10^6/100$ μl PBS per mouse) *via* the right flank. After 7 days, when the tumour diameters were about 0.5 cm, the mice were randomly divided into three groups (five per group) for daily intra-tumour injection of liposomal miR-26b mimics (5 μg/100 μl), liposomal miR-26b mimics control (5 μg/100 μl) and PBS (100 μl as blank) for 28 days. The tumour volume was monitored, and calculated using the formula: $V = 1/2 \times$ larger diameter $\times$ (smaller diameter)^2. Growth curves were plotted using average tumour volume and tumour weight at the set time-points. The tumour dimensions were recorded for 28 days, after which the mice were killed. The dissected tumours were fixed in neutral buffered formalin and embedded in paraffin, and sections (5 μm) were prepared for immunohistochemistry and histological examination..

Immunohistochemistry and histological examination

For immunohistochemistry, the sections were deparaffinized and rehydrated, and then antigen retrieval was carried out by boiling the samples in citrate buffer for 15 min. at 92°C to 98°C and trypsinizing with 0.125% trypsin (Invitrogen) for 15 min. at 37°C. The sections were immersed in 3% hydrogen peroxide and distilled water for 30 min. to block endogenous peroxidase activity. Non-specific staining was eliminated by a 20 min. incubation with normal sheep serum (DAKO Corp., Heverlee, Belgium). The sections were incubated with rabbit anti-human proliferating cell nuclear antigen (PCNA) antibody (1:125 dilution) (Abcam, Cambridge, CA, USA) or rabbit anti-human CD31 antibody (1:50) (Santa Cruz Biotechnology, Santa Cruz, CA, USA) at 37°C for 2 hrs, and then incubated with goat anti-rabbit secondary antibodies (IgG/HRP) (Zhongshan Goldenbridge Biotechnology Corp., Beijing, China) for 15 min. at 37°C using Non-Bio Two-Step Histostain™-Plus kits, DAB staining (Zhongshan Goldenbridge Biotechnology Corp.). The nuclei were counterstained with haematoxylin. The remaining procedures were performed in accordance with the manufacturer's instructions.

For histological examination, the sections were stained with haematoxylin and eosin.

Both immunohistochemical stained and haematoxylin and eosin stained sections were observed by light microscopy (Olympus Optical Co., Lake Success, NY, USA).

Prediction of miRNA targets

Identification of miRNA targets is critical for investigation of the functions of miRNAs. Currently, a majority of studies have employed computational programs to predict gene targets and then validate these targets using experimental methods. Three different computational programs, TargetScan (http://www.targetscan.org/) [39], PicTar (http://pictar.bio.nyu.edu.) [40] and miRanda (http://www.microrna.org/) [41] have been employed to predict miRNA targets. In the present study, three discrete lists of the predicted targets were first generated by TargetScan, PicTar and miRanda. After the three lists were generated by the three computational programs, a fourth list was generated which contained only the genes predicted by the three initial computational programs.

Differential genes between LoVo and NCM460 cell lines

Cells of a normal human colon epithelial cell line, NCM460, which was derived from non-transformed colonic epithelial cells [42] and provided by INCELL Corporation (San Antonio, TX, USA) as part of an active research collaboration. The NCM460 cells were cultured in an M3 base medium (INCELL Corporation) supplemented with 10% FBS and 1% antibiotic–antimycotic as previously described [43].

The Illumina data obtained from the LoVo and NCM460 cell lines were extracted using software provided by the manufacturer, and normalized using the 'normalize.quantiles' function, the genes with significant different expression levels between LoVo and NCM460 cell lines were identified as calculated by the statistical analysis with a *P*-value <0.01, and then only those genes with 2-fold or more changes in the expression intensity were selected for gene intersection following analysis.

Intersection of genes between the differentially expressed genes between LoVo and NCM460 cell lines and the prediction of gene targets of miR-26b

Intersection of analyses of genes led to genes selected from the differentially expressed genes between LoVo and NCM460 cell lines and from the prediction of miRNA targets was carried out by TargetScan (http://www.targetscan.org/) [39], PicTar (http://pictar.bio.nyu.edu.) [40], and miRanda (http://www.microrna.org/) [41].

Prediction and analysis of the genes and network pathways associated with metastasis

MetaCore™ is a web-based computational platform that provides analysis of gene clusters in the context of regulatory networks and signalling pathways, and thus is used for system biology and drug discovery. In the present study, Network analyses of differentially expressed genes were performed by using the MetaCore™ Analytical suite (GeneGo, Inc., St. Joseph, MI, USA). MetaCore™ was also used to calculate the statistical significance based on the probability of assembly from a random set of nodes of the same size as the input list. To build the network of differentially expressed miRNAs and genes, we applied the shortest paths algorithm to establish directed paths between the selected objects.
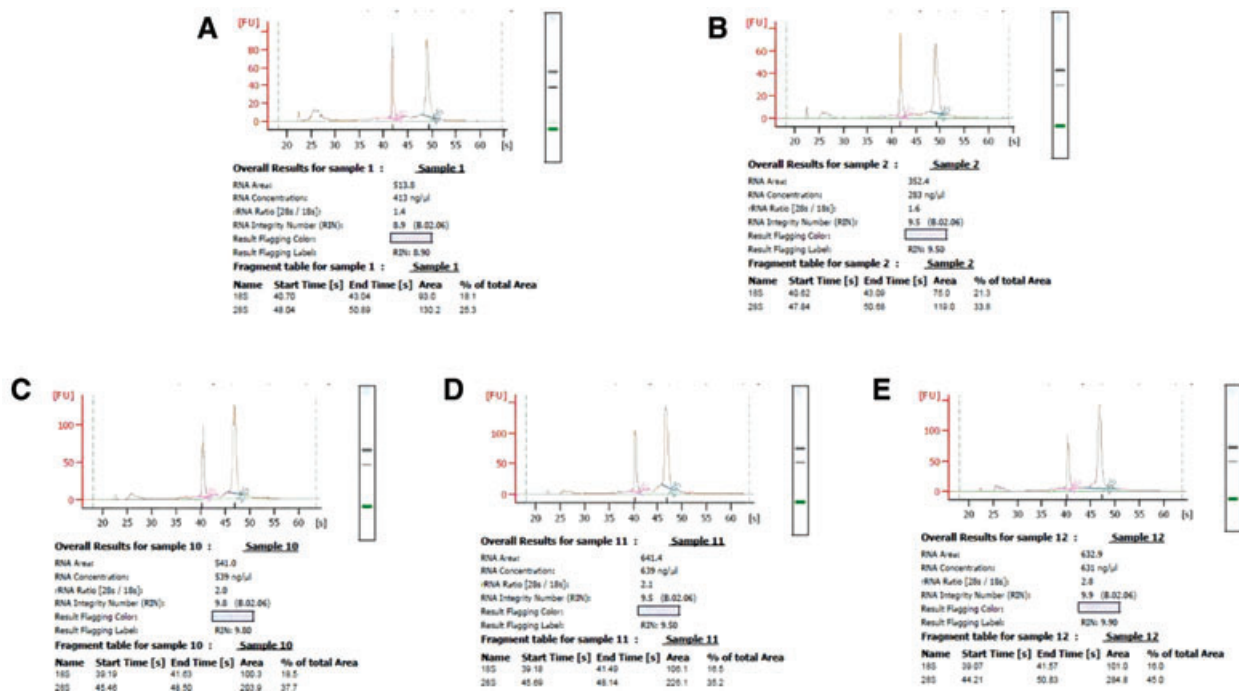
Fig. 1 Total RNA was quantified and tested by microfluidic analysis.

Statistical analysis

Statistical analyses were performed by GraphPad Prism software (GraphPad Prism Software, Version 5.01, GraphPad, San Diego, CA, USA). All quantitative data were recorded as mean $\pm$ standard deviation (S.D.). Comparisons between two groups were performed by Student's t-test or Wilcoxon two-sample test, where appropriate, and comparisons among multiple groups were performed by ANOVA. Statistical significance was defined as $P < 0.05$.

Results

Differentially expressed miRNAs among HUES-17, LoVo, SW480, HT29 and Caco-2 cell lines

The integrity of RNA isolated in each group was excellent, with the ratio of absorbance of total RNA at OD260/280 nm of 1.8–2.2. Electrophoresis indicated high quality of the extracted RNA (Fig. S1). In order to acquire the reliable and precise data on miRNAs, the total RNA was quantified and tested as a quality control for high quality RNA (Fig. 1). Differentially expressed patterns of miRNAs were observed among the five different cell lines. A total of 659 out of the 875 currently known human miRNAs were detected in the five different cell lines (Fig. 2). Of

these 659 miRNAs, 497 were detected in HUES-17 cells, 364 in LoVo cells, 378 in SW480 cells, 352 in HT29 cells and 428 in Caco-2 cells. The expression levels were low for a majority of the detected miRNAs; 518 miRNAs gave signals less than 500. However, 118 miRNAs were expressed with signals higher than 1000; some were expressed with signals even higher than 20,000.

miRNAs that had similar expression patterns in HUES-17 and LoVo cell lines, but were significantly different from the patterns in the other three cell lines with a low metastatic potential were identified. Accordingly, eight miRNAs, miR-26b, miR-1246b, let-7e, miR-21, miR-196a, miR-16–2*, miR-1180 and miR-15b*, were identified as differentially expressed among the cell lines ($P < 0.05$). Among these miRNAs, miR-26b was further investigated as the P-value was less than 0.01 (Table 1 and Fig. 3).

Confirmatory and validation studies on differentially expressed miRNA(s) by qRT-PCR

To confirm the microarray results, the most notable differentially expressed miRNA, miR-26b, was investigated by qRT-PCR.The miR-26b relative intensity (RI; mean $\pm$ S.D.) levels varied among the test cells. They were lowest in HUES-17 (0.35 ± 0.02) and LoVo (1.04 ± 0.08) cells, which were significantly different from each other. The miR-26b levels among Caco-2 (2.93 ± 0.09), HT-29 (2.28 ± 0.24) and SW480 (3.25 ± 0.16) cells were not significantly different from each other. The combined level of
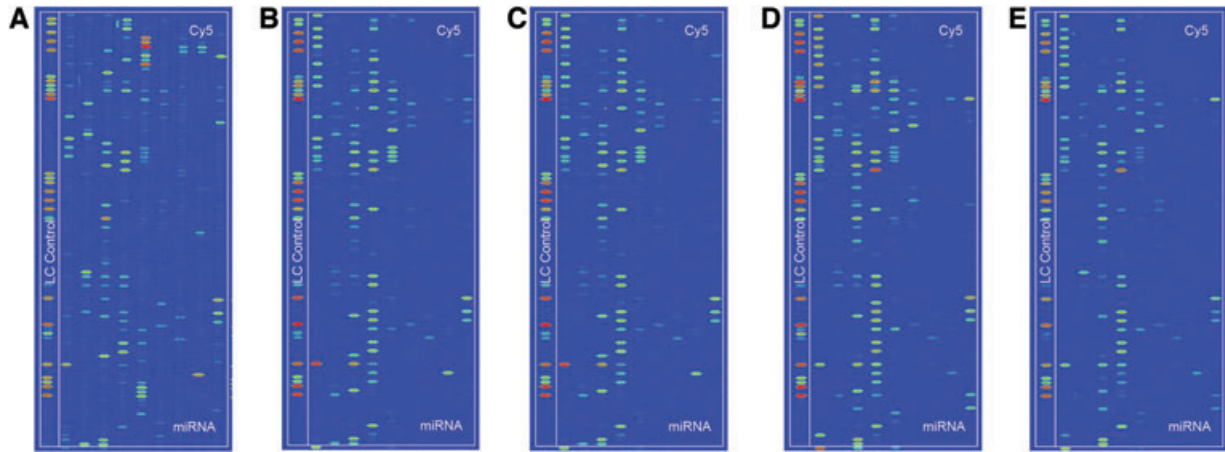
Fig. 2 Differentially expressed miRNAs. Differentially expressed patterns of miRNAs in the five different cell lines of HUES-17 (**A**), LoVo (**B**), SW480 (**C**), HT29 (**D**), Caco-2 (**E**).

Table 1 Eight miRNAs (miR-26b, miR-1246b, let-7e, miR-21, miR-196a, miR-16–2*, miR-1180 and miR-15b*) with the similar expression pattern between hESC and LoVo cell lines (LoVo with the highest potentiality of metastasis), but significantly different with the other three CRC cells: SW480, HT-29 and Caco-2 with the low potentiality of metastasis

| Reporter name	H17 (A)	LOVO (B)	SW480 (C)	HT-29 (D)	CACO-2 (E)	AB (G2)	CDE (G1)	Log2 (G2/G1)	*P*-value
hsa-miR-26b	1081	1030	6390	7323	6571	1056 ± 36	6761 ± 495	2.68	6.68E-04
hsa-miR-1246	25,009	29,733	10,817	12,333	14,699	27,371 ± 3340	12,616 ± 1956	-1.12	2.44E-02
hsa-let-7e	91	171	5738	13,446	1764	131 ± 57	6983 ± 5940	5.74	3.09E-02
hsa-miR-21	15,443	13,361	34,079	30,291	22,791	14,402 ± 1472	29,054 ± 5745	1.01	3.85E-02
hsa-miR-196a	5	24	5475	1494	619	14 ± 14	2529 ± 2588	7.47	3.89E-02
hsa-miR-16–2*	40	36	85	71	93	38 ± 3	83 ± 11	1.13	1.59E-02
hsa-miR-1180	70	57	319	151	279	64 ± 9	250 ± 87	1.97	3.42E-02
hsa-miR-15b*	30	18	74	133	128	24 ± 9	112 ± 33	2.24	4.11E-02
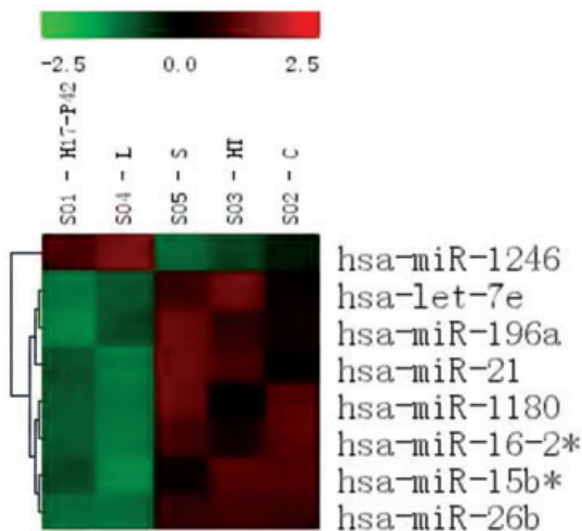
Fig. 3 Comparisons of select miRNAs in cell lines. Identification of miRNAs whose normalized expression patterns are lower in a hESC line (HUES-17) and a CRC cell line (LoVo) with metastatic potentiality, compared to three other CRC cell lines (SW480, HT-29 and Caco-2) with low metastatic potential. Accordingly, eight miRNAs (miR-26b, miR-1246b, let-7e, miR-21, miR-196a, miR-16–2*, miR-1180 and miR-15b*) were identified as differentially expressed miRNAs with a *P*-value of <0.05. Furthermore, miR-26b was identified as the most notable differentially expressed miRNA with a *P*-value of <0.01.
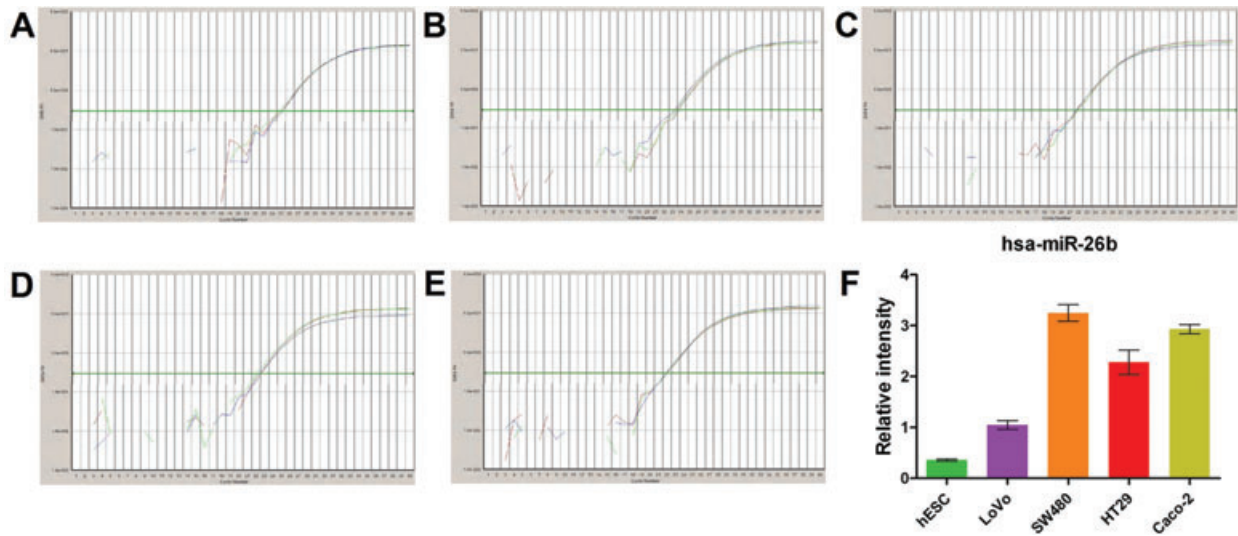
Fig. 4 Comparisons of miRNA-26b expression in tested cell lines by QRT-PCR. (**A**) Different cell lines, HUES-17, LoVo, Caco-2, HT-29 and SW480, are shown as each amplification curve for miR-26b. (**B**). After subtraction and normalization of the background, different levels of miR-26b are calculated by the ΔCT method, and the relative expression levels are converted into $2^{-\Delta CT}$ method as shown in the chart. The miR-26b expression levels between HUES-17 and LoVo cells are similar. There was no significant difference in miR-26b expression levels among Caco-2, HT-29 and SW480 cells. However, the levels of miR-26b are higher in SW480, HT-29, Caco-2 cells than those in HUES-17, and LoVo cells. Values represent the mean $\pm$ S.D. of three independent experiments, each run in triplicate.

miR-26b in HUES-17 and LoVo cells was significantly lower than that in SW480, HT-29 and Caco-2 cells (0.72 ± 0.31 *versus* 2.28 ± 0.22, $P = 0.02$) (Fig. 4).

To validate the microarray finding, miR-26b expression in CRC, adenoma and tumour adjacent 'normal' tissues collected from patients was determined by qRT-PCR. The level of miR-26b was lower in the CRC tissues (0.65 ± 0.10) than in the 'normal' colorectal tissues (1.09 ± 0.12). However, there was no significant difference in the miR-26b expression between the CRC and adenoma tissues (Fig. 5).

Effects of miR-26b mimics on human colorectal cancer cell proliferation and apoptosis *in vitro*

The fluorescence signal was observed in LoVo cells 48 hrs after the cells were transfected with the miR-26b mimics control as shown in Figure 6A. RT-PCR assay showed that miR-26b expression was significantly increased in miR-26b mimics-transfected cells when compared with the other three groups (miR-26b mimics control, liposome control and PBS control, Fig. 6B). No apparent increase in miR-26b expression was observed by simultaneous transfection of miR-26b mimics control.

In the clonogenic formation assay, upon 14-day continuous culture, the clone number in miR-26b mimics group was lower than that in the miR-26b mimics control group (Fig. 6C).

In LoVo cells, miR-26b mimics induced apoptosis in 34.75% of cells, whereas the rates were 18.22% in PBS control group,

22.41% of liposome control group and 23.78% in mimics control groups (Fig. 6D).

Effects of miR-26b on human colorectal cancer cell migration and invasion *in vitro*

In a cell migration assay, transient transfection with miR-26b mimics significantly inhibited cell migration, with mean number of migrated cells of 10.00 ± 2.00), compared with the values in other three groups (PBS control: 32.00 ± 5.29; mimics control: 36.67 ± 4.51; and liposome control: 30.67 ± 5.13, Fig. 6E). Similarly, transient transfection with miR-26b mimics also inhibited LoVo cell invasion; the mean number of invasive cells was 8.33 ± 1.53 in miR-26b mimics group, whereas the values 13.67 ± 2.08 in PBS control; 18.00 ± 2.65 in mimic control and 12.33 ± 3.51 in liposome group) in a cell invasion assay (Fig. 6F).

Effects of miR-26b on tumour xenograft growth, cell proliferation and histological changes *in vivo*

To study the anti-tumorigenic role of miR-26b in CRC, immunodeficient BALB/C mice were subcutaneously inoculated with human LoVo colon cancer cells and housed until the tumour cells, initially loosely distributed in matrigel. Tumour was generated in all animals after inoculation of with human LoVo colon cancer cells. No death or signs of possible toxicity were observed during the study
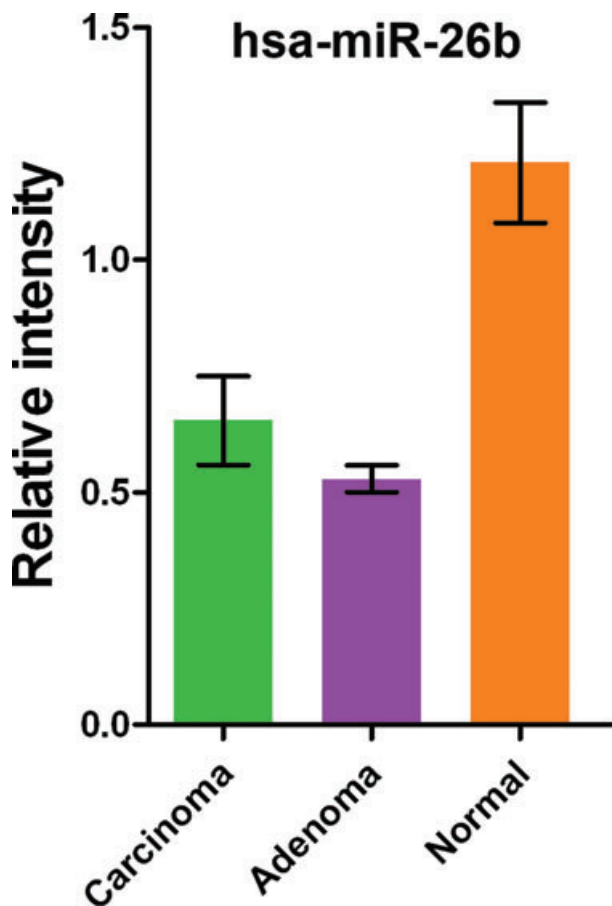
Fig. 5 Detection of hsa-miR-26b in fresh clinical tissue isolates. Confirmatory studies on miRNA-26b expression in clinical colorectal samples by QRT-PCR. After background subtraction and normalization, different levels of miR-26b were calculated by the ΔCT method and the relative expression levels are converted into $2^{-\Delta CT}$ method as shown in the chart. The level of miR-26b was lower in both the colorectal carcinoma and adenoma tissues compared to normal colorectal tissues. There was no significant difference in miR-26b levels between CRC and adenoma tissues. Values represent the mean $\pm$ S.D. of three independent patient samples, each run in triplicate.

period of time. Although the initial volumes of tumours were approximately equal of all mice, significant differences in tumour growth were observed during the treatment, as illustrated by the tumour growth curve in Figure 7A. Over the course of treatment, all tumour volumes increased, but the tumours in mice treated with miR-26b mimics presented significantly lower growth rates in comparison with those treated with PBS and miR-26b mimics control at the end of the experiment. Furthermore, the decrease of tumour volumes was observed after 24 days of miR-26b mimics treatment. At the termination of the experiment, the tumour volume in mice treated with miR-26b mimics was 387.97 $\pm$ 84.07 mm^3, which was significantly smaller than those in mice treated with PBS (416.94 $\pm$ 144.47 mm^3) and miR-26b mimics control (489.64 $\pm$ 84.67 mm^3). Also, the tumour weight in mice

treated with miR-26b mimics was 0.40 $\pm$ 0.05 g, which was significantly lighter than those in mice treated with PBS (0.44 $\pm$ 0.06 g) and miR-26b mimics control (0.48 $\pm$ 0.03 g).

Histological analysis revealed that tumours treated with miR-26b mimics control or PBS were densely packed with viable LoVo cells and only contained small necrotic areas occasionally (Fig. 7B, left and right panels). These necrotic areas were likely due to the aggressive nature of LoVo cells that rapidly outgrew other cancer cells and competed for blood supply and nutrients [44]. In contrast, tumours treated with miR-26b mimics contained large areas that were filled with necrotic cell debris (Fig. 7B, centre panel), and enlarged necrotic cores, which suggest that miR-26b inhibited cell proliferation and accelerated the cell death in tumour samples. The different necrotic degrees of tumours among the three groups are also shown in the gross pictures (Fig. 7B).

As shown in Figure 7B, the relative expression intensity of PCNA$^+$ and CD31$^+$ cells in mice treated with miR-26b mimics were lower than in mice treated with PBS or miR-26b mimics control. In addition, no significant effects on proliferation were observed between PBS and control groups.

Prediction and validation of the gene targets of miR-26b

To explore the potential functions of miR-26b, we employed three computational programs (TargetScan, PicTar and miRanda) to predict the targets of miR-26b. After the three lists of miR-26b-targeted genes predicted by TargetScan, PicTa and miRanda were systematically analysed, the most promising 77 candidate targeted genes for miR-26b were listed in Table S1. The expression levels of differentially expressed genes between LoVo and NCM460 cell lines were analysed by the statistical analysis with a P-value of <0.05. A total of 583 differentially expressed genes with 2-fold or more changes in the expression intensity between the two cell lines were selected for further analysis (Table S2). To further validate the true gene targets of miR-26b, four genes (TAF12, PTP4A1, CHFR and ALS2CR2) among the differentially expressed genes between LoVo and NCM460 cell lines, were also predicted by the miRNA targets by TargetScan, PicTar and miRanda (Fig. 8).

Prediction and analysis of the genes and network pathways associated with tumorigenesis and progression

Raw microarray data were imported into MetaCore™ for integrate network analysis. Eight miRNAs (miR-26b, miR-1246b, let-7e, miR-21, miR-196a, miR-16–2*, miR-1180 and miR-15b*) with differentially expressed were extrapolated using an intersection algorithm. The regulatory pathways were found to be significantly associated with tumorigenesis and progression of CRC cells. As shown in Figure 9, functional network analysis revealed that the

Fig. 6 miR-26b expression correlates with cell proliferation inhibition and apoptosis induction. Ectopic expression of miR-26b and its effects on cell proliferation, apoptosis, migration and invasion of miR-26b mimics-transfected LoVo cells *in vitro*. (**A**) LoVo cells transfected with the miR-26b mimics control oligonucleotide double strands labelled with a fluorescein amidite molecule attached at its 5′OH end. The fluorescence signal is observed 48 hrs after the transfection under a fluorescence (a) or optical (b) microscope. (**B**) qRT-PCR assay showing that miR-26b expression is increased in miR-26b mimics-transfected cells but not the other control groups (miR-26b mimics control, liposome control and PBS control). (**C**) Clonogenic formation assay showing that the clone numbers is decreased miR-26b mimics-transfected cells (a), compared with miR-26b mimics controls-transfected cells (b). (**D**) Annexin V/PI staining assay showing apoptosis is increased in miR-26b mimics-transfected cells compared with the other three groups (miR-26b mimics control, liposome control and PBS control). (**E**) Cell migration assay showing that cell migration is inhibited for miR-26b mimics-transfected cells. (**F**) Cell invasion assay showing that cell migration is inhibited for miR-26b mimics-transfected cells.
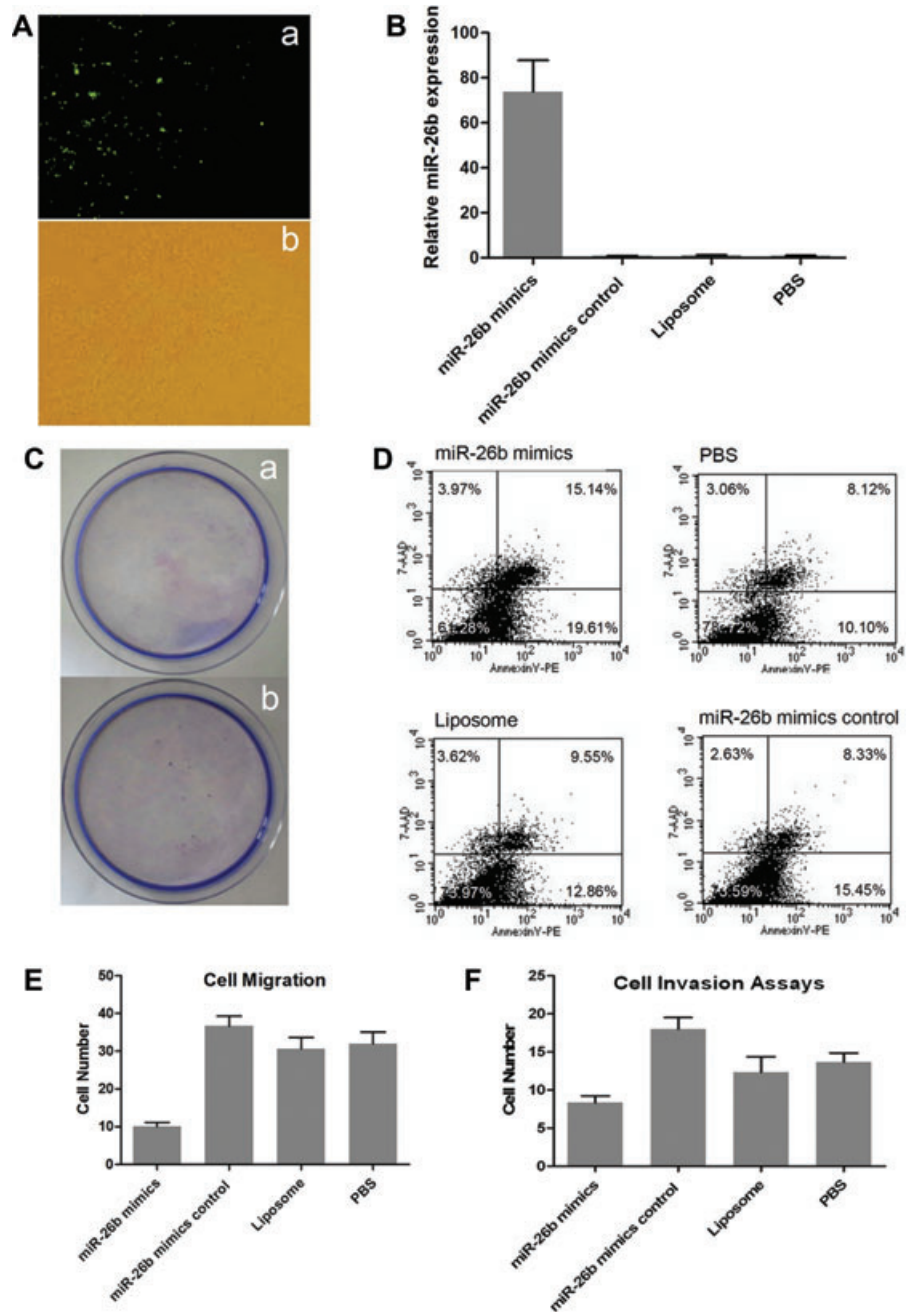
expression of the six miRNAs was indirectly interacted with each other through the related oncogenes, tumour suppressor genes or genes encoding transcriptional factors. The indirect interactions among the differentially expressed miRNAs and the related genes, the localizations and edges of differentially expressed miRNAs and the related genes in the functional network pathway, and the functional pathways of differentially expressed miRNAs and related genes in the regulatory pathways analysis by MetaCore are shown in Tables S3–5. miR-26b directly interacted with c-Myc, P-53 and interleukin (IL)-6, and also indirectly with the metastasis gene STAT3 (Fig. 9).

Discussion

The finding represents the first report of the remarkable activity of miR-26b both *in vitro* and *in vivo* against human CRC, particularly
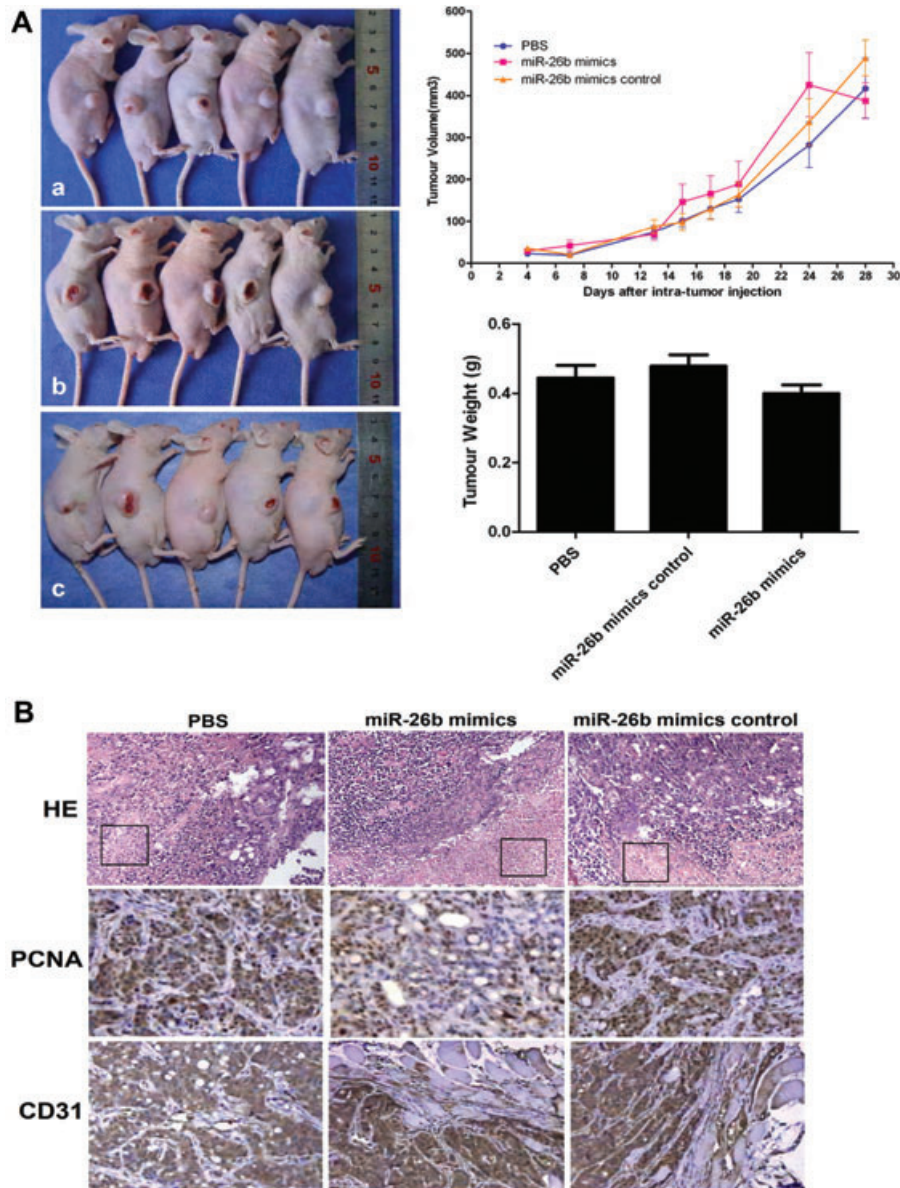
Fig. 7 Effects of miR-26b mimics on growth and histology of established colon tumour xenografts. (**A**) Left panel: images of mice carrying LoVo tumours on day 28. Upper right panel: tumour volume growth curve after intra-tumour injection of miR-26b mimics, miR-26b mimics control or PBS over the study period. After day 24, miR-26b mimics (b) treatment resulted in a significantly decrease in tumour growth, compared with control of PBS (a) or miR-26b mimics control (c). Lower right panel: tumour weights of three groups measured on day 28. (**B**) Tumour histological examination and immunohistochemical staining specific for PCNA and CD31. Haematoxylin and eosin indicates the area containing necrotic cells, cell debris or cells undergoing cell necrosis.

metastatic tumour cells, and suggests that miR-26b may also have a role in embryonic cell growth and regulation. It has been documented that some molecules that are expressed at high levels in foetal tissues, such as carcinoembryonic antigen (CEA), alpha-fetoprotein (AFP), glypican-3 and nucleophosmin (NPM) [45], are also highly expressed in human tumour tissues, but seldom expressed in the normal tissues in the adult; thus these genes and proteins are shared in the processes of embryogenesis and tumorigenesis [46]. It has been suggested that the initiation of embryonic implantation is associated with the acquisition of an invasive cellular phenotype, which comprises a host of cellular processes that include expression or repression of specific cell adhesion molecules, elaboration of matrix-digesting enzymes and acquisition of a blood supply [28]. Genes and proteins that regulate this pathway are generally dormant in the adult, but could be reinitiated when cellular invasion is part of the phenotype seen in cancer cells, particularly as they metastasize.

Tumours employ many of the same methods to grow and spread as first used by cytotrophoblasts. Like the trophoblasts, tumour cells migrate through and invade their surrounding ECM. Access to the vasculature and recruitment of a blood supply, which are hallmarks of both early embryos and tumours, are needed to achieve exponential growth patterns [28]. Based on this theory, we carried out this study to determine if we could find dif-
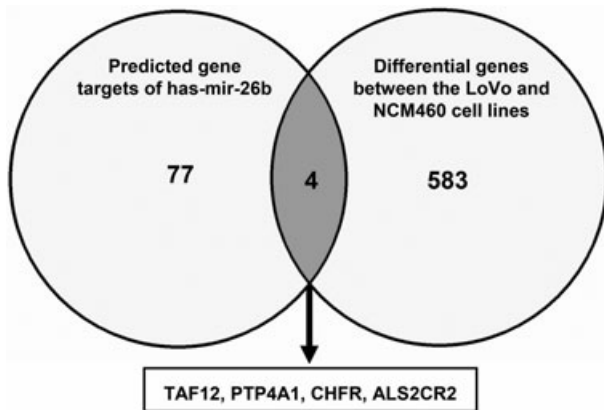
Fig. 8 Prediction and validation of the gene targets of miR-26b.

ferentially expressed miRNAs in a hESC line, HUES-17, and a highly metastatic tumour line LoVo, relative to other CRC cell lines with the lower metastatic potential.

In the present study, eight miRNAs, miR-26b, miR-1246b, let-7e, miR-21, miR-196a, miR-16–2*, miR-1180 and miR-15b*, were identified as differentially expressed in HUES-17 and LoVo cells, compared with SW480, HT-29 and Caco-2 cells ($P < 0.05$). However, only one of the miRNAs (*i.e.* miR-26b) was found to be most notable differentially expressed ($P < 0.01$). qRT-PCR further confirmed the results of microarray analysis and that the expres-

sion levels of miR-26b were significantly lower in HUES-17 and LoVo cells than in SW480, HT-29 and Caco-2 cells. Meanwhile, miR-26b expression was assessed in fresh tissue isolates of CRC, adenoma and normal colorectal tissues collected from CRC patients was determined by qRT-PCR, which showed that the expression level of miR-26b was lower in the CRC tissues than in the normal colorectal tissues.

The present data clearly indicated that overexpression of miR-26b by miR-26b mimics transfection inhibited cell proliferation and induced cell apoptosis *in vitro*. Transwell assays confirmed that miR-26b inhibited the *in vitro* migration and invasion of the metastatic human CRC cell line LoVo. Moreover, we observed the effects of miR-26b overexpression on a tumour xenograft model. It was noteworthy that, consistent with the outcome obtained *in vitro*, overexpression of miR-26b mimics *in vivo* resulted in decreased tumour growth, accompanied with inhibition of cell proliferation and cell death. In addition, no changes in gross measures, such as weight loss, feeding, behaviour or other signs of possible side effects, were observed during against CRC, which provides us with an attractive approach for further investigation.

To explore the potential functions of miR-26b, the targets genes of miR-26b were predicted by the computational programs PicTar, TargetScan and miRanda [39–41]. Meanwhile, the expression levels of differentially expressed genes between LoVo and NCM460 cell lines were also analysed, and 583 differentially expressed genes were selected for further analysis. To further determine the true gene target of miR-26b, intersection of

Fig. 9 Functional network analysis of miRNAs and genes associated with tumour invasiveness and metastasis. (**A**) The network was generated by a shortest paths algorithm of MetaCore (GeneGo, Inc.) software using the eight differentially expressed miRNAs (*i.e.* miR-26b, miR-1246b, let-7e, miR-21, miR-196a, miR-16–2*, miR-1180 and miR-15b*). Individual miRNAs and genes are represented as nodes, and the different shapes of the nodes represent the functional class of the miRNAs and genes. The edges define the relationships among the nodes: the arrowheads indicate the direction of the interaction. The regulatory pathways with eight differentially expressed miRNAs were extrapolated by using an intersection algorithm, which were found to be associated with CRC invasiveness and metastasis. Six miRNAs indirectly interact with each other through the related oncogenes, tumour suppressor genes or genes encoding transcriptional factors. miR-26b directly interacts with c-Myc, p53 and IL-6 and indirectly with the metastasis gene, STAT3. (**B**) Annotations of symbols and abbreviations in the regulatory network.
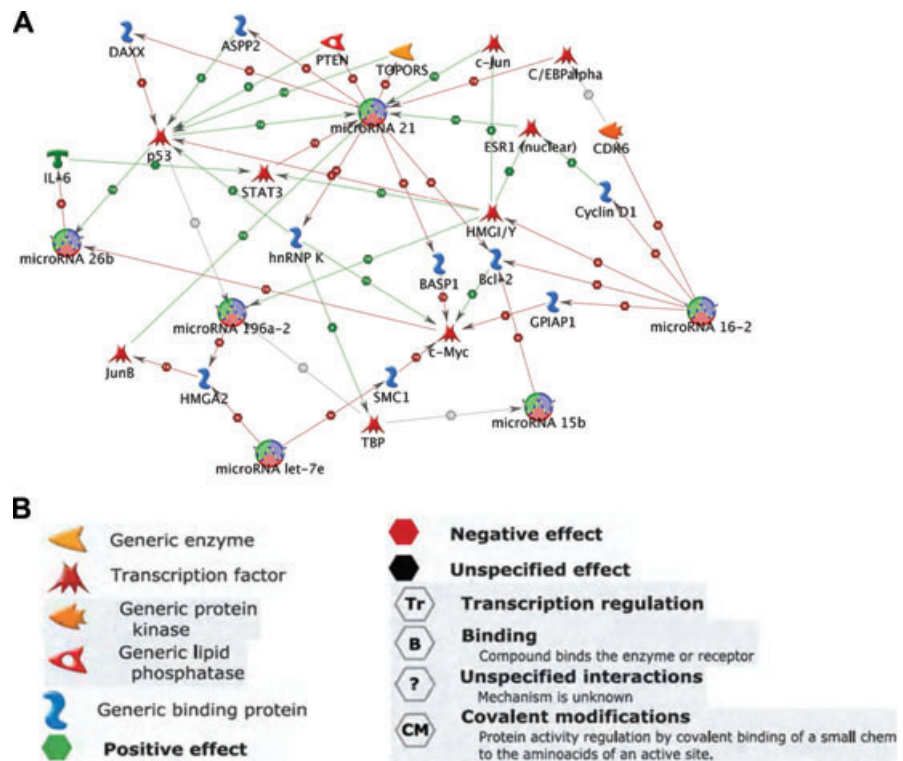
four genes (TAF12, PTP4A1, CHFR and ALS2CR2) were identified among those differentially expressed genes. Therefore, miR-26b might be involved in the regulation of multiple biological progresses by targeting cancer-related genes, genes encoding transcriptional factors, stress-associated genes and other functional genes.

MetaCore is a web-based computational platform that includes a curetted database of human miRNA, gene, protein interactions and metabolism, and thus is a useful tool for analysing a cluster of miRNAs or genes in the context of regulatory networks and signalling pathways [47–50]. Ekins *et al.* [51], using only eight differentially expressed miRNAs as input, showed that the 'Analyze network' algorithm was useful in providing additional information that was not present in the original list of root nodes. In the present study, functional network analysis using the MetaCore database demonstrated the most directly target cancer-related genes of miRNA-26b, as well as other differentially miRNAs. In addition, six of the differentially expressed miRNAs were shown to indirectly contact and interact with each other by genes encoding transcriptional factors, stress-associated genes or other functional genes.

Down-regulation of miR-26b has been observed in head, neck and oral cancers [52–53]. Interestingly, the expression of miR-26 family members have been shown to be induced by hypoxia [54] but down-regulated by exposure to cigarette smoke [55]. The Myc oncogene suppresses miR-26a, another member of the miR-26 family, which influences cell cycle progression by targeting the oncogene EZH2 in a murine lymphoma model [56]. Liver tumours with low miR-26 expression are distinct from those with high miR-26 expression in transcriptome activities and are associated with poor survival [57]. Many of the genes that are overexpressed in tumours with reduced miR-26 expression are related to cell immunity, such as those encoding pro-inflammatory and anti-inflammatory cytokines [57]. Moreover, many signalling networks that are activated in tumours with low miR-26 expression are immune-associated, such as NF-κB–IL-6, IL-10 and STAT3 pathways [58]. Our results from the functional network analysis using the MetaCore database were in concert with these observations.

In conclusion, miR-26b is identified to be the most notable differentially expressed miRNA in HUES-17 and LoVo cells, compared with SW480, HT-29 and Caco-2 cells. Overexpression of miR-26b expression by miR-26 mimics transfection inhibits cell proliferation, migration and invasion, and induces apoptosis of CRC LoVo cells *in vitro*, and inhibits tumour growth *in vivo*. Four genes (TAF12, PTP4A1, CHFR and ALS2CR2) are identified to be the targets of miR-26b. These data suggested that miR-26b might serve as a novel prognostic factor and possibly an attractive therapy for CRC. The lack of toxicity during the *in vivo* treatment period in the xenograft test models, suggests that treatment with miR-26b mimics was safe and without detectable toxicity, further supporting a rationale for pursuing miR-26b as a promising novel therapeutic target.

Conflict of interest

None of the authors of this study has any applicable conflict of interest.

Supporting Information

Additional Supporting Information may be found in the online version of this article:

Fig. S1 Total RNA separated with 1% agarose gel electrophoresis in the five different cell lines (hESC, LoVo, Caco-2, HT-29, SW480).

Table S1 The most promising 77 candidate targeted genes for miR-26b were predicted by TargetScan, PicTa and miRanda

Table S2 583 differential genes with 2-fold or more changes in expression intensity between the LoVo and NCM460 cells group

Table S3 The indirect interaction with each other between the differentially expressed microRNAs and the related genes

Table S4 The localizations and edges of differentially expressed microRNAs and the related genes in the functional network pathway

Table S5 The functional pathway of differentially expressed microRNAs and related genes in the regulatory pathways analysis by MetaCore

Please note: Wiley-Blackwell are not responsible for the content or functionality of any supporting materials supplied by the authors. Any queries (other than missing material) should be directed to the corresponding author for the article.

References

1. **Carthew RW, Sontheimer EJ.** Origins and mechanisms of miRNAs and siRNAs. *Cell.* 2009; 136: 642–55.

2. **Schramke V, Allshire R.** Hairpin RNAs and retrotransposon LTRs effect RNAi and chromatin-based gene silencing (Retracted Article. See vol 301, p. 1069, 2003). *Science.* 2003; 301: 1069–74.

3. **Noma K, Sugiyama T, Cam H, et al.** RITS acts in cis to promote RNA interference-mediated transcriptional and post-transcriptional silencing. *Nat Genet.* 2004; 36: 1174–80.

4. **Kim VN, Han J, Siomi MC.** Biogenesis of small RNAs in animals. *Nat Rev Mol Cell Bio.* 2009; 10: 126–39.

5. **Hagen JW, Lai EC.** microRNA control of cell-cell signaling during development and disease. *Cell Cycle.* 2008; 7: 2327–32.

6. **Winter J, Jung S, Keller S, et al.** Many roads to maturity: microRNA biogenesis pathways and their regulation. *Nat Cell Biol.* 2009; 11: 228–34.

7. **Esquela-Kerscher A, Slack FJ.** Oncomirs – microRNAs with a role in cancer. *Nat Rev Cancer.* 2006; 6: 259–69.

8. **Alvarez-Garcia I, Miska EA.** MicroRNA functions in animal development and human disease. *Development.* 2005; 132: 4653–62.

9. **Bartel DP.** MicroRNAs: genomics, biogenesis, mechanism, and function. *Cell.* 2004; 116: 281–97.

10. **Fidler IJ.** Timeline – The pathogenesis of cancer metastasis: the 'seed and soil' hypothesis revisited. *Nat Rev Cancer.* 2003; 3: 453–8.

11. **Weigelt B, Peterse JL, van't Veer LJ.** Breast cancer metastasis: markers and models. *Nat Rev Cancer.* 2005; 5: 591–602.

12. **Gupta GP, Massague J.** Cancer metastasis: building a framework. *Cell.* 2006; 127: 679–95.

13. **Tavazoie SF, Alarcon C, Oskarsson T, et al.** Endogenous human microRNAs that suppress breast cancer metastasis. *Nature.* 2008; 451: 147–52.

14. **Batlle E, Sancho E, Franci C, et al.** The transcription factor Snail is a repressor of E-cadherin gene expression in epithelial tumour cells. *Nat Cell Biol.* 2000; 2: 84–9.

15. **Cano A, Perez-Moreno MA, Rodrigo I, et al.** The transcription factor snail controls epithelial-mesenchymal transitions by repressing E-cadherin expression. *Nat Cell Biol.* 2000; 2: 76–83.

16. **Yang J, Mani SA, Donaher JL, et al.** Twist, a master regulator of morphogenesis, plays an essential role in tumor metastasis. *Cell.* 2004; 117: 927–39.

17. **Hartwell KA, Muir B, Reinhardt F, et al.** The Spemann organizer gene, Goosecoid, promotes tumor metastasis. *P Natl Acad Sci USA.* 2006; 103: 18969–74.

18. **Mani SA, Yang J, Brooks M, et al.** Mesenchyme Forkhead 1 (FOXC2) plays a key role in metastasis and is associated with aggressive basal-like breast cancers. *P Natl Acad Sci USA.* 2007; 104: 10069–74.

19. **Ma L, Teruya-Feldstein J, Weinberg RA.** Tumour invasion and metastasis initiated by microRNA 10b in breast cancer. *Nature.* 2007; 449: 682-U2.

20. **Seligson DB, Horvath S, Shi T, et al.** Global histone modification patterns predict risk of prostate cancer recurrence. *Nature.* 2005; 435: 1262–6.

21. **Lim LP, Lau NC, Garrett-Engele P, et al.** Microarray analysis shows that some microRNAs downregulate large numbers of target mRNAs. *Nature.* 2005; 433: 769–73.

22. **He L, Thomson JM, Hemann MT, et al.** A microRNA polycistron as a potential human oncogene. *Nature.* 2005; 435: 828–33.

23. **Johnson SM, Grosshans H, Shingara J, et al.** RAS is regulated by the let-7 MicroRNA family. *Cell.* 2005; 120: 635–47.

24. **Calin GA, Croce CM.** MicroRNA signatures in human cancers. *Nat Rev Cancer.* 2006; 6: 857–66.

25. **Lu J, Getz G, Miska EA, et al.** MicroRNA expression profiles classify human cancers. *Nature.* 2005; 435: 834–8.

26. **Roldo C, Missiaglia E, Hagan JP, et al.** MicroRNA expression abnormalities in pancreatic endocrine and acinar tumors are associated with distinctive pathologic features and clinical behavior. *J Clin Oncol.* 2006; 24: 4677–84.

27. **Ma YL, Peng JY, Liu WJ, et al.** Proteomics identification of desmin as a potential oncofetal diagnostic and prognostic biomarker in colorectal cancer. *Mol Cell Proteomics.* 2009; 8: 1878–90.

28. **Murray MJ, Lessey BA.** Embryo implantation and tumor metastasis: common pathways of invasion and angiogenesis. *Semin Reprod Endocr.* 1999; 17: 275–90.

29. **Hanahan D, Weinberg RA.** The hallmarks of cancer. *Cell.* 2000; 100: 57–70.

30. **Monzo M, Navarro A, Bandres E, et al.** Overlapping expression of microRNAs in human embryonic colon and colorectal cancer. *Cell Res.* 2008; 18: 823–33.

31. **Hatfield SD, Shcherbata HR, Fischer KA, et al.** Stem cell division is regulated by the microRNA pathway. *Nature.* 2005; 435: 974–8.

32. **Houbaviy HB, Murray MF, Sharp PA.** Embryonic stem cell-specific MicroRNAs. *Dev Cell.* 2003; 5: 351–8.

33. **Farh KKH, Grimson A, Jan C, et al.** The widespread impact of mammalian microRNAs on mRNA repression and evolution. *Science.* 2005; 310: 1817–21.

34. **Wu Z, Zhang W, Chen GB, et al.** Combinatorial signals of Activin/Nodal and bone morphogenic protein regulate the early lineage segregation of human embryonic stem cells. *J Biol Chem.* 2008; 283: 24991–5002.

35. **Gao XL, Gulari E, Zhou XC.** In situ synthesis of oligonucleotide microarrays. *Biopolymers.* 2004; 73: 579–96.

36. **Bolstad BM, Irizarry RA, Astrand M, et al.** A comparison of normalization methods for high density oligonucleotide array data based on variance and bias. *Bioinformatics.* 2003; 19: 185–93.

37. **Eisen MB, Spellman PT, Brown PO, et al.** Cluster analysis and display of genome-wide expression patterns. *P Natl Acad Sci USA.* 1998; 95: 14863–8.

38. **Doench JG, Petersen CP, Sharp PA.** siRNAs can function as miRNAs. *Genes Dev.* 2003; 17: 438–42.

39. **Lewis BP, Shih IH, Jones-Rhoades MW, et al.** Prediction of mammalian microRNA targets. *Cell.* 2003; 115: 787–98.

40. **Krek A, Grun D, Poy MN, et al.** Combinatorial microRNA target predictions. *Nature Genetics.* 2005; 37: 495–500.

41. **Sethupathy P, Megraw M, Hatzigeorgiou AG.** A guide through present computational approaches for the identification of mammalian microRNA targets. *Nat Methods.* 2006; 3: 881–6.

42. **Moyer MP, Manzano LA, Merriman RL, et al.** NCM460, a normal human colon mucosal epithelial cell line. *In Vitro Cell Dev Biol Anim.* 1996; 32: 315–7.

43. **Zhao D, Keates AC, Kuhnt-Moore S, et al.** Signal transduction pathways mediating neurotensin-stimulated interleukin-8 expression in human colonocytes. *J Biol Chem.* 2001; 276: 44464–71.

44. **Edinger AL, Thompson CB.** Death by design: apoptosis, necrosis and autophagy. *Curr Opin Cell Biol.* 2004; 16: 663–9.

45. **Lee NPY, Leung KW, Cheung N, *et al.*** Comparative proteomic analysis of mouse livers from embryo to adult reveals an association with progression of hepatocellular carcinoma. *Proteomics.* 2008; 8: 2136–49.

46. **Hendrix MJC, Seftor EA, Seftor REB, *et al.*** Reprogramming metastatic tumour cells with embryonic microenvironments. *Nat Rev Cancer.* 2007; 7: 246–55.

47. **Dezso Z, Nikolsky Y, Sviridov E, *et al.*** A comprehensive functional analysis of tissue specificity of human gene expression. *Bmc Biol.* 2008; 6: 49.

48. **Ekins S, Nikolsky Y, Bugrim A, *et al.*** Pathway mapping tools for analysis of high content data. *Methods Mol Biol.* 2007; 356: 319–50.

49. **Dezso Z, Nikolsky Y, Nikolskaya T, *et al.*** Identifying disease-specific genes based on their topological significance in protein networks. *Bmc Syst Biol.* 2009; 3: 36.

50. **Tsai MS, Hwang SM, Chen KD, *et al.*** Functional network analysis of the transcriptomes of mesenchymal stem cells derived from amniotic fluid, amniotic membrane, cord blood, and bone marrow. *Stem Cells.* 2007; 25: 2511–23.

51. **Ekins S, Bugrim A, Brovold L, *et al.*** Algorithms for network analysis in systems-ADME/Tox using the MetaCore and MetaDrug platforms. *Xenobiotica.* 2006; 36: 877–901.

52. **Wong TS, Liu XB, Wong BYH, *et al.*** Mature miR-184 as potential oncogenic microRNA of squamous cell carcinoma of tongue. *Clin Cancer Res.* 2008; 14: 2588–92.

53. **Kozaki KI, Imoto I, Mogi S, *et al.*** Exploration of tumor-suppressive microRNAs silenced by DNA hypermethy-lation in oral cancer. *Cancer Res.* 2008; 68: 2094–105.

54. **Kulshreshtha R, Ferracin M, Wojcik SE, *et al.*** A microRNA signature of hypoxia. *Mol Cell Biol.* 2007; 27: 1859–67.

55. **Izzotti A, Calin GA, Arrigo P, *et al.*** Downregulation of microRNA expression in the lungs of rats exposed to cigarette smoke. *FASEB J.* 2009; 23: 806–12.

56. **Sander S, Bullinger L, Klapproth K, *et al.*** MYC stimulates EZH2 expression by repression of its negative regulator miR-26a. *Blood.* 2008; 112: 4202–12.

57. **Ji JF, Shi J, Budhu A, *et al.*** MicroRNA expression, survival, and response to interferon in liver cancer. *New Engl J Med.* 2009; 361: 1437–47.

58. **Thyrell L, Arulampalam V, Hjortsberg L, *et al.*** Interferon alpha induces cell death through interference with interleukin 6 signaling and inhibition of STAT3 activity. *Exp Cell Res.* 2007; 313: 4015–24.